



ORIGINAL ARTICLE

Construction of a QCM sensor for detecting diethylstilbestrol in water based on the computational design of molecularly imprinted polymers



Xuhong Cai ^a, Junbo Liu ^{a,*}, Dadong Liang ^a, Shanshan Tang ^{b,*}, Bao Xu ^c

^a College of Resource and Environment, Jilin Agricultural University, Changchun, Jilin 130118, China

^b College of Life, Key Laboratory of Straw Comprehensive Utilization and Black Soil Conservation, The Ministry of Education, Jilin Agricultural University, Changchun, Jilin 130118, China

^c Institute of Mathematica, Jilin Normal University, Siping, Jilin 136000, China

Received 16 October 2022; accepted 15 January 2023

Available online 20 January 2023

KEYWORDS

Diethylstilbestrol;
Quartz crystal microbalance;
Molecular imprinting
polymers

Abstract Combining molecular imprinting technology and quartz crystal microbalance (QCM), the diethylstilbestrol-molecularly imprinted polymers (DES-MIPs) were designed. The LC- ω PBE/6-31G(*d,p*) method was chosen to predict the properties of DES-MIPs in this study. The calculated results showed that the complex formed from DES and methacrylic acid with molar ratio of 1:5 and ethylene dimethacrylate as cross-linking agent had the largest amount of hydrogen bonds, the lowest binding energy, and the optimal stability property. With the guidance of calculations, the DES-MIPs were used to prepare QCM electrode by embedding method to construct the DES-MIPs-QCM sensor. The experimental results displayed that the sensor had a high binding affinity for DES when the DES-MIPs was 15 mg and the coating volume was 10 μ L. The minimum detection limit of the sensor for DES was 2.63 ng/mL in the range of 50 to 350 ng/mL. The DES-MIPs-QCM sensor exhibited high recognition capacity for DES compared to its structural analogs. The sensor had been successfully used for the determination of DES in the actual water samples.

© 2023 The Author(s). Published by Elsevier B.V. on behalf of King Saud University. This is an open access article under the CC BY-NC-ND license (<http://creativecommons.org/licenses/by-nc-nd/4.0/>).

* Corresponding authors at: College of Resource and Environment, Jilin Agricultural University, Changchun 130118, China (J. Liu).

E-mail addresses: liujb@ccut.edu.cn (J. Liu), tangshanshan81@163.com (S. Tang).

Peer review under responsibility of King Saud University.



Production and hosting by Elsevier

1. Introduction

Diethylstilbestrol (DES) is a synthetic lipophilic estrogen that has been widely used in the treatment of functional bleeding, infertility, and osteoporosis caused by hormonal imbalance (Craig and Keating, 2022). However, with the unregulated use of DES as a growth-promoting feed additive in livestock and poultry farming, trace residues of DES in environmental water bodies are widespread (Jiang et al., 2012). Because DES is more stable and not easily degraded, it

accumulates in the body through the food chain and leads to an increase in the rate of hermaphroditism, sex ratio disorders, and reproductive organ mutations (Giusti et al., 1995; Jiang et al., 2016; Sweeney et al., 2015), and also increases the risk of breast cancer, endometrial cancer, and vaginal cancer in women (Huo et al., 2017; Troisi et al., 2018; Troisi et al., 2019; Upson et al., 2015). The use of DES as a growth promoter in livestock was prohibited early in the United States and the European Union (Zhang et al., 2008). In China, the applications of DES and its esters in animal-derived food were also banned in 2002 (Mi et al., 2019).

Currently, the main methods for analysis and detecting trace DES of environment are high-performance liquid chromatography (He et al., 2016), liquid chromatography-tandem mass spectrometry (Guo et al., 2013; Hu et al., 2014), and pressurized capillary electrochromatography (Liu et al., 2005). However, the adsorption between traditional solid-phase extraction sorbent and the target is non-selective in all the detection methods. Thus, the extractions of different analytes and matrices required the selection of different sorbent packings. Moreover, the elution conditions also should be strictly selected. The long analysis period, high cost, and cumbersome steps limited the widely use of the above assay methods. Therefore, it is especially important to develop the assay methods with high selectivity, rapid detection, and good stability to detect the DES contaminant residues in water bodies.

The molecularly imprinted quartz crystal microbalance (QCM) sensor is a sensitive detector which uses the piezoelectric effect of quartz crystal to indirectly measure nanogram-level weight changes on the electrode surface (Czanderna and Lu, 1984). This method is widely used in many fields, including environmental monitoring (Eddaif et al., 2020; Qi et al., 2021), food inspection (Chi and Liu, 2022), and drug analysis (Fuji et al., 2022), due to its benefits in terms of simple operation, sensitive response, strong selectivity, stability, and online detection. To obtain better selectivity, the molecularly imprinted polymers (MIPs) with a defined arrangement of binding sites are fixed on the crystal electrode surface of the QCM sensor (Fang et al., 2016a, 2016b; Fang et al., 2017; Kong et al., 2014; Latif et al., 2014). The MIPs are as the recognition component of electrode to construct the molecularly imprinted QCM sensor. The mass-based molecularly imprinted QCM sensors are based on the mass change, which is caused by the adsorbed determinand on the surface of quartz crystal. Thus, the bonding and recognition processes of the determinand on the recognition part of MIPs are the keys to the analytical measurement. In order to obtain the maximum response and minimum interference when the sensor detects DES pollutants with low concentration in complex matrix environment, it is particularly important to prepare DES-MIPs with higher selectivity and adsorption. There are few literatures related to the screening of functional monomers, imprinting ratios, and cross-linking agents for DES imprinting systems combining theoretical and experimental studies. Moreover, there is no research on DES-MIPs-QCM sensors. In recent years, more and more researchers have used quantum chemical computational methods such as LC- ω PBE (Nayyar et al., 2011) and M062X (Liu et al., 2022) to simulate and design molecularly imprinted polymers. Here, the functional monomer, imprinting ratio, and cross-linking agent had been optimized by simulating the DES molecular imprinting self-assembly system. Then, under the guidance of simulated computational data, the DES-MIPs-QCM sensor using the DES-MIPs modified quartz crystal electrodes had been constructed. The detection performance of the sensor for ultra-low residual DES in environmental water had also been investigated.

2. Materials and methods

2.1. Reagents and Instruments

DES, estrone (E1, standards), estriol (E3, standards), bisphenol A (BPA, standards), and ethylene dimethacrylate (EDMA,

analytically pure) were purchased from Shanghai Aladdin Reagent Co., Ltd. Methacrylic acid (MAA, analytically pure), azobisisobutyronitrile (AIBN, analytically pure), acetonitrile (analytically pure), methanol (analytically pure), acetic acid (analytically pure), and tetrahydrofuran (analytically pure) were purchased from Tianjin Guangfu Fine Chemical Research Institute. Polyvinyl chloride (PVC, S-1000) was acquired from the China Petrochemical Corporation, Qilu Branch. The Quartz Crystal Microbalance Analyzer (CHI400C) was purchased from Shanghai Chenhua Instruments Co., Ltd. The Scanning Electron Microscope (JSM-5600), JEOL Electronics Co., Japan. Constant temperature water bath (HH-S) was purchased from Shanghai Boxun Industrial Co. Vacuum drying oven (TDL-60B) was purchased from Shanghai Anting Technology Instrument Factory.

2.2. Calculation method

All calculations were performed by using the Gaussian 09 program version A.02 software (Frisch et al., 2009). With the 6-31G(*d,p*) basis set, the geometric configuration of the template molecule DES (Fig. 1) was optimized by M062X, B3LYP, CAM, LC- ω PBE, PBE1PBE, and ω B97XD, respectively (Parr, 1983). The frequency calculations were performed at the same level, and the default value is used for convergence.

The optimized calculation method was used to optimize the molecular geometry configuration of four functional monomers, namely, MAA, acrylamide (AM), 3-aminophenylboronic acid (APBA), and *o*-phenylenediamine (OPD), respectively. The imprinted binding sites of DES and the four different monomers were first analyzed based on the natural bonding orbital (NBO) charges and molecular electrostatic potential (MEP). Then all the isomeric structures of the template-monomer complexes with varying ratios between DES and the four functional monomers had been optimized in order to determine the best functional monomer and the optimal molar ratio. The binding energy (ΔE_1) between DES and functional monomer was calculated by equation (1), and the basis set iterative addition error was corrected using the counterpoise procedure (CP) method proposed by Boys and Bornardi (Aqababa et al., 2013).

$$\Delta E_1 = E_{CP} - E_{DES} - \sum E_{Monome} \quad (1)$$

E_{CP} (kJ/mol) is the total energy of the template-monomer complex. E_{DES} (kJ/mol) is the energy of DES. $\sum E_{Monome}$ (kJ/mol) is the sum of the functional monomer energies.

The binding energy (ΔE_2) of MAA functional monomer and crosslinker at a molar ratio of 1:1 is calculated as follows:

$$\Delta E_2 = E_{CP} - E_{MAA} - E_{CA} \quad (2)$$

E_{CP} (kJ/mol) is the energy of complex (1:1) formed from MAA and crosslinker. E_{MAA} (kJ/mol) is the energy of MAA. E_{CA} (kJ/mol) is the energy of the crosslinker.

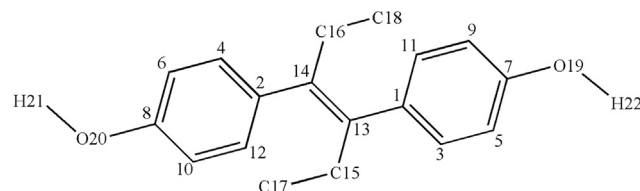


Fig. 1 The molecular structure of DES.

2.3. Preparation of DES-MIPs and NIPs

Based on the theoretical calculation results, DES-MIPs and NIPs were prepared. 0.5 mmol DES was dissolved in 50 mL acetonitrile solvent, and the corresponding functional monomers were added according to the optimal imprinting ratio between template and monomer. The pre-polymerization reaction of template and monomer was performed after ultrasound for 1 h. A certain amount of EDMA (reaction ratio between monomer and cross-linking agent was 1:5) and 0.15 g AIBN were added to the above sample solution with ultrasonic dissolving method. After deoxygenation, the mixed solution was sealed and precipitated polymerized in the constant temperature water bath at 60 °C for 24 h. The color of solution changed from colorless to milky white during the reaction process. After reaction finished, the solution was dried in the vacuum drying oven at 40 °C to obtain DES-MIPs. The DES-MIPs were extracted by soxhlet extraction using a methanol/acetic acid solution (v/v, 9/1) for 48 h to completely remove template molecules DES in the DES-MIPs. Then the methanol was used to elute DES in the DES-MIPs for 24 h until the eluate was neutral. The samples were dried again in the vacuum drying oven to constant weight in order to obtain the MIPs without template molecule DES. The preparation process of NIPs was the same as that of MIPs, except no template was added.

2.4. Construction of DES-MIPs- QCM electrodes

The QCM sensor was mainly consisted by a detection cell, an oscillator, a converter, a piezoelectric quartz crystal electrode, and a computer system. The quartz crystal electrode is the key section of the QCM sensor. It is used the DES-MIPs as the identification component. DES molecularly imprinted QCM electrodes were constructed by a certain amount DES-MIPs (NIPs) and 10 mg PVC, which were placed in 10 mL of tetrahydrofuran reagent. The fundamental frequency of piezoelectric quartz crystal electrode for QCM sensor was 8 MHz, and its diameter was 8 mm. After ultrasound for 60 min, the mix-solution was dropwise added to the middle of the QCM electrode in order to make the liquid evenly spread on the electrode surface. The DES-MIPs (NIPs) modified molecularly imprinted QCM electrodes were obtained after tetrahydrofuran volatilized. The modified electrode was fixed in the detection cell. When the modified film of electrode surface adsorbed DES substrate, the frequency of piezoelectric quartz crystal substrate would change along with the change of electrode mass. By detecting the frequency change of electrode output signal, the quantitative detection of determinand can be realized. The equations are as follow.

$$\Delta f = f_i - f_0 \quad (3)$$

$$\Delta f = -2.26 \times 10^{-6} f_0^2 \Delta m / A \quad (4)$$

Δf (Hz) is the value of the frequency change of the crystal substrate. f_i (Hz) is the response frequency after frequency stabilization. f_0 (Hz) is the fundamental frequency of the crystal substrate. Δm (g) is the amount of binding of DES-MIPs (NIPs) to DES. A (0.205 cm²) is the dial area of the crystal surface of electrode.

After each test, the electrode was removed, and the modified film on the electrode surface was eluted with methanol-

acetic acid eluent (v/v,7:3) and double-distilled water. The cleaning procedure was repeated more than 5 times. When the response frequency is the reference frequency, it means that the modified film has been eluted cleanly. That is to say, the residues of DES in the actual samples should be nearly zero. The electrode is dried under N₂ atmosphere and then stored in a dry box for backup. The diagram of DES molecularly imprinted QCM electrode construction was shown in Fig. 2.

2.5. Detection condition optimization of DES molecularly imprinted QCM sensors

In order to obtain the maximum sensitivity of electrode for the DES molecularly imprinted QCM when detecting the actual water sample, the different additions (5, 7.5, 10, 12.5, 15, 17.5, and 20 mg) of DES-MIPs (NIPs) and coating amounts (5, 10, 15, 20, and 25 μL) had been investigated, respectively. According to the response frequency of the QCM sensor, the optimal addition and coating amounts of DES-MIPs were determined.

2.6. Study of DES selectivity

The response frequencies of DES, E3, E1, and BPA solutions (200 ng/mL) were measured by using the sensor when E3, E1, and BPA were selected as competing molecules (Fig. 3). All measurements were repeated three times, the average values were taken, and the selection factor (α) was calculated.

$$\alpha = \Delta F_{\text{DES}} / \Delta F_A \quad (5)$$

ΔF_{DES} (Hz) is the value of the frequency change of the sensor response to the template molecule DES. ΔF_A (Hz) is the value of the frequency change of the sensor response to competing molecules E3, E1, and BPA.

2.7. Application of sensors in environmental sample detection

The water sample (5 L, Blue Lake of Jilin Agricultural University) was filtered and heat concentrated to 10 mL. The concentrated sample and 5 mL DES standard solution (50 and 200 ng/mL) were placed in a 30 mL centrifuge tube. After ultrasound for 15 min, the mix-solution was left for 6 h. The supernatant of mix-solution was filtered with a 0.22 μm filter tip. 20 μL determinand solution was added to the background solution using a micropipettor, and the response values of DES were recorded using the constructed QCM sensor.

3. Results and discussion

3.1. Selection of theoretical calculation methods

Table 1 lists the bond lengths and bond angle values of DES optimized by the different methods (M062X, B3LYP, CAM, LC- ω PBE, PBE1PBE, and ω B97XD) with 6-31G(*d,p*) basis set and corresponding experimental crystal data (Yearley et al., 2008). As can be seen from Table 1, the geometrical structure parameters of DES calculated by the six theoretical calculation methods (M062X, B3LYP, CAM, LC- ω PBE, PBE1PBE, and ω B97XD) were very close to each other and were within the error tolerance. The standard deviations of

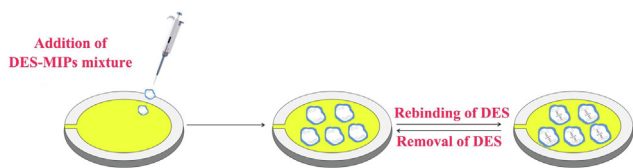


Fig. 2 The diagram of DES molecularly imprinted QCM electrode construction.

bond lengths calculated by the six methods were 0.0003, 0.0004, 0.0012, 0.0003, 0.0005 and 0.0004 nm, and the standard deviations of bond angles were 1.2610, 1.2847, 1.2555, 1.2243, 1.3162 and 1.2626°, respectively. Compared with the other five methods, the standard deviation values of the structural parameters calculated by the LC- ω PBE method were the smallest, indicating that the geometrical parameters calculated under the LC- ω PBE theory could be in good agreement with the experimental values. Thus, the LC- ω PBE/6-31G(*d,p*) method was chosen to optimize the geometrical configuration of DES, functional monomers, and their complexes in this study. Moreover, the LC- ω PBE/6-31G(*d,p*) method could also give the satisfactory forecast results in the other studies (Vydrov and Scuseria, 2006; Sarghein et al., 2022).

3.2. MEP and NBO analysis

In order to determine the bonding sites between DES and four functional monomers (AM, APBA, MAA, and OPD), the NBO charges and MEP were calculated. The active site of action of molecule could be predicted by the NBO charges of the atom. Moreover, the molecule could be a proton donor (proton acceptor) when it owned positively charged (negatively

charged). As can be seen from Fig. 4(a), the O atoms (O19, O20) in the phenolic hydroxyl groups of DES have more negative charges, which are both -0.695 . The H atoms in the benzene rings and phenolic hydroxyl groups of DES own the more positive charges, which are $+0.495$ (H21, H22), $+0.243$ (H26, H28), and $+0.261$ (H23, H29), respectively. Among them, O19, O20, H21, and H22 atoms on the phenolic hydroxyl group have larger absolute values of charge, and they are the most important active sites of DES. Similarly, the main active sites of AM (Fig. 4(b)) are O2 (-0.604) in the carbonyl group and H4 ($+0.429$) and H5 ($+0.420$) in the amine group. The main active sites of APBA (Fig. 4(c)) are N11 (-0.865), H12 ($+0.405$), and H13 ($+0.406$) on the amine group and O15 (-0.901), O17 (-0.898), H16 ($+0.494$), and H18 ($+0.494$) on the hydroxyl group. The main active sites of MAA (Fig. 4(d)) are O6 (-0.601) on the carbonyl group and H8 ($+0.512$) on the hydroxyl group. The main active sites of OPD (Fig. 4(e)) are N11 (-0.888), N12 (-0.888), H13 ($+0.410$), H14 ($+0.405$), H15 ($+0.410$), and H16 ($+0.405$) on the amine group. As seen from Fig. 4, the electrostatic potential in different regions of DES and the four monomer molecules are shown by different colors. The red area indicates the electron-rich region with electrophilic activity, i.e., the positively charged particles have strong interactions with it. The blue area indicates the electron-deficient region with nucleophilic activity, i.e., the negatively charged particles are easily approached by it. It is clear that O atoms on the hydroxyl and carbonyl groups and N atoms on the amine groups of the five compounds are more electronegative and surrounded by a higher density of electron clouds, making them vulnerable to attack by electrophilic reagents. H atoms on the benzene ring, hydroxyl group, and amine group have high electrostatic positive potentials and are easily attacked by nucleophilic

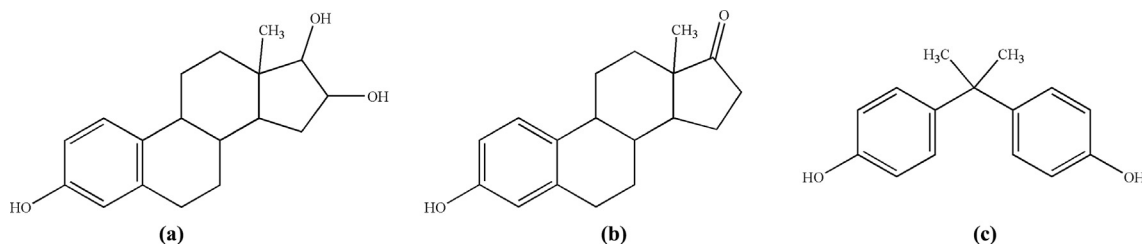


Fig. 3 Molecular structures of E3 (a), E1 (b), and BPA (c).

Table 1 Structural parameters of DES calculated using M062X, B3LYP, CAM, LC- ω PBE, PBE1PBE, and ω B97XD methods, and corresponding experimental data (Exp.).

Species	M062X	B3LYP	CAM	LC- ω PBE	PBE1PBE	ω B97XD	Exp.
<i>R</i> (nm)							
C2-C12	0.1397	0.1402	0.1395	0.1391	0.1410	0.1396	0.1389
C4-C6	0.1388	0.1391	0.1396	0.1383	0.1397	0.1387	0.1391
C6-C8	0.1395	0.1399	0.1393	0.1391	0.1406	0.1395	0.1382
C8-C10	0.1394	0.1397	0.1391	0.1389	0.1405	0.1394	0.1380
C10-C12	0.1392	0.1395	0.1420	0.1388	0.1401	0.1392	0.1395
Φ (°)							
C2-C12-C10	121.31	121.48	121.42	121.40	121.50	121.33	120.86
C2-C4-C6	121.50	121.73	121.64	121.58	121.78	121.52	121.73
C4-C6-C8	119.67	119.76	119.72	119.74	119.78	119.74	119.23
C10-C8-O20	122.74	122.87	122.76	122.71	122.97	122.82	121.97

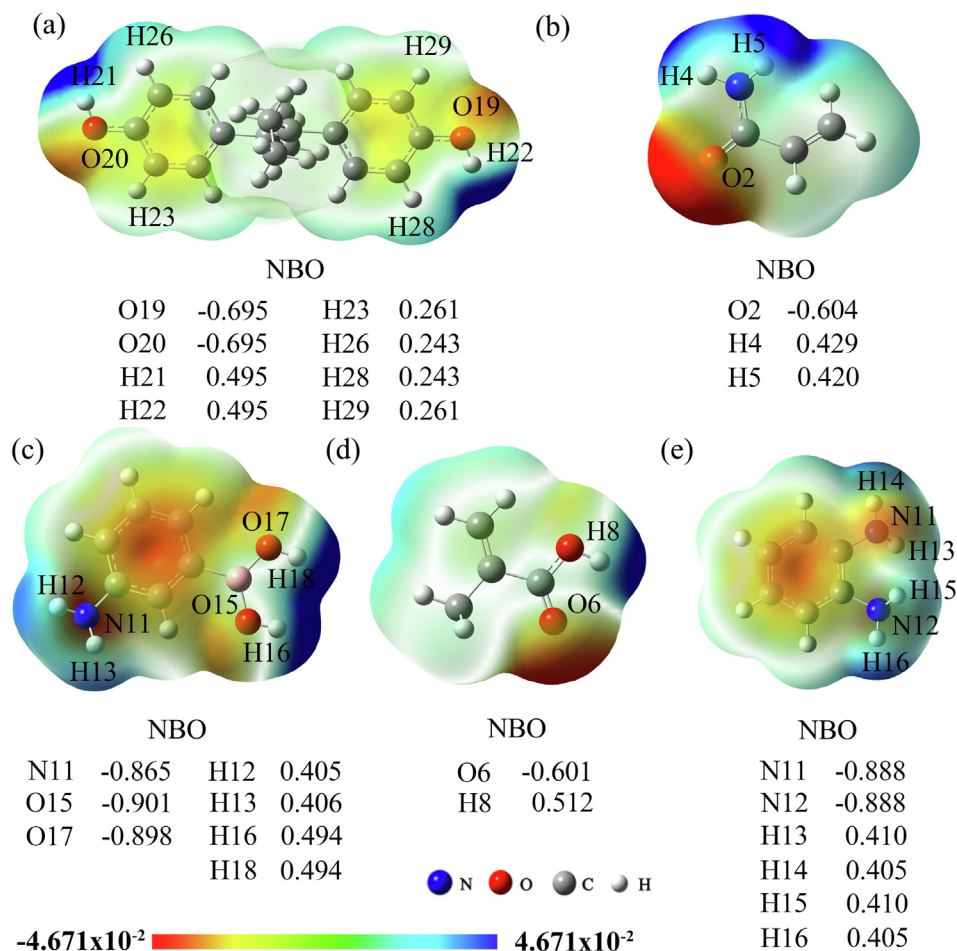


Fig. 4 MEP distributions and NBO charges of DES (a), AM (b), APBA (c), MAA (d), and OPD (e).

reagents. The results of MEP analysis were consistent with those of NBO charges analysis.

3.3. Optimization of the functional monomer

The imprinted polymers have the special ability, which is remembering the template molecule. It is because that the imprinted pores of MIPs are spatially arranged in a regular rule, and MIPs have special functional groups which could interact with template molecule. Thus, the selection of functional monomers for imprinting is crucial. In the synthesis of MIPs, the largest the molar ratio between template molecules and monomers is, the more favorable the recognition of the imprinted pores with shape and spatial structure in MIPs. The important factors affecting the pore shape and spatial structure are the selection of the functional monomer and molar ratio. The stable spatial configurations of complexes formed from DES and four functional monomers (AM, APBA, OPD, and MAA) were simulated at the LC- ω PBE/6-31G(*d,p*) level, respectively. In Fig. 5 and Table 2, the DES-MAA stable complex had the largest molar ratio, the largest amount of hydrogen bonds, and the lowest binding energy, which means that the MAA could be expected to prepare MIPs with higher adsorption, better selectivity, and more stability. In addition, from Fig. 5(d) and Table 2, one can find that O19 and O20 in DES acted as electron donors to form

double hydrogen bonds with electron acceptors H60 (H72) and H48 (H84) in MAA, respectively. The formation of these double hydrogen bonds greatly increased the stability of the prepolymer. In summary, DES and MAA formed a prepolymer with the largest molar ratio (1:5), the highest amount of binding bonds (9), and the highest stability. It could be expected to synthesize DES-MIPs with the highest imprinting efficiency.

3.4. Screening of the cross-linking agent

For the specified imprinted molecules, the imprinting efficiency and recognition ability of MIPs are influenced not only by the type of functional monomer and the imprinting ratio but also by the type of cross-linking agent. To improve the imprinting efficiency of MIPs to DES template molecules and the stability of the imprinted polymer, the binding energy between the selected crosslinker and MAA functional monomer should be as low as possible, however, it should be higher than that between DES and MAA functional monomer (Khan et al., 2015). Fig. 6 shows the binding energies (ΔE_2) between MAA and DES and between MAA and two crosslinkers (DVB and EDMA), respectively, with a molar ratio of 1:1. As shown in Fig. 6, the binding energy (ΔE_2) between MAA and DVB (EDMA) was -13.67 (-29.70) kJ/mol, which were both higher than that of DES-MAA complex with a molar

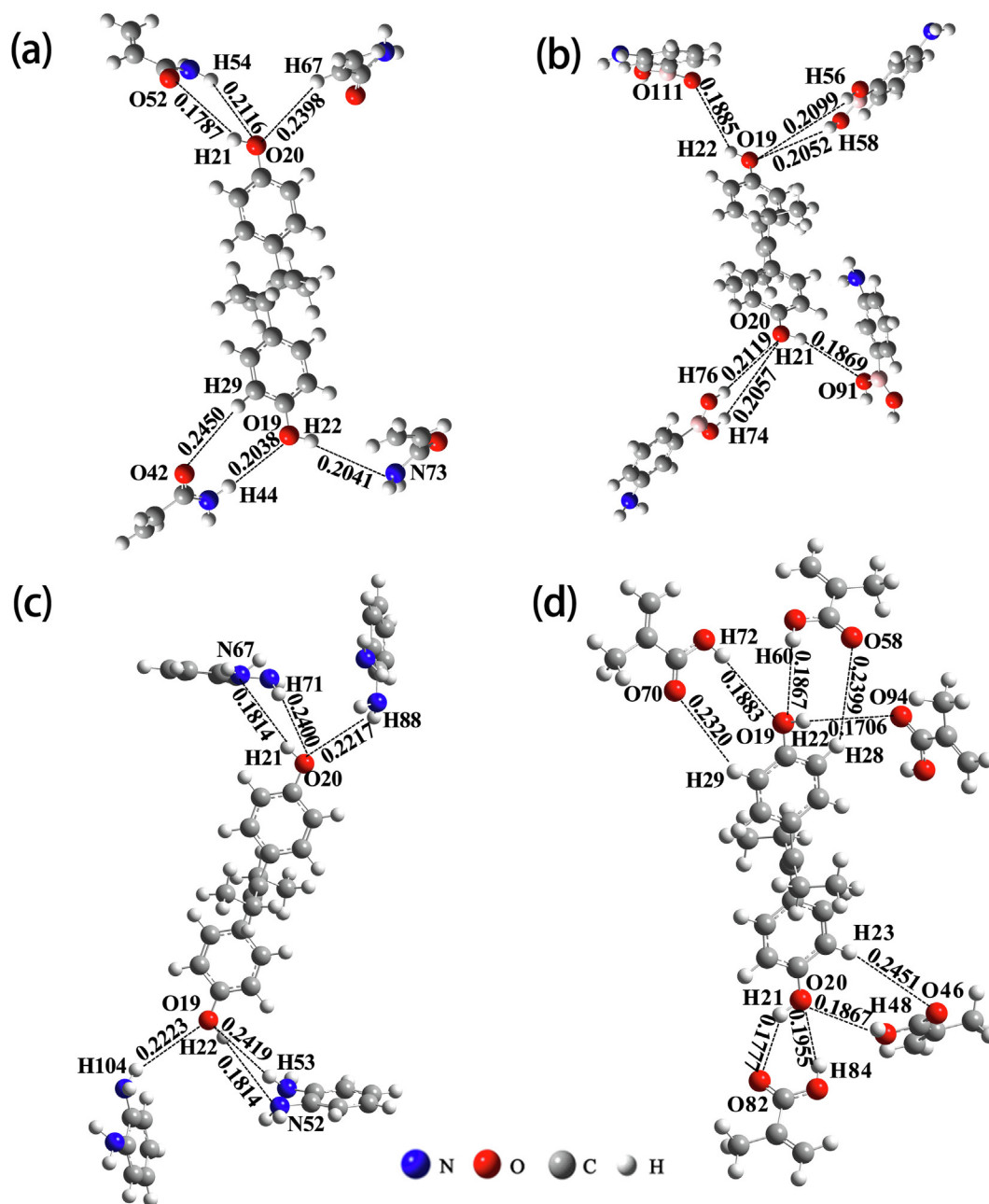


Fig. 5 Models of complexes formed from template molecules and functional monomers: (a) DES-AM (1:4); (b) DES-APBA (1:4); (c) DES-OPD (1:4); (d) DES-MAA (1:5).

ratio of 1:1 (-41.08 kJ/mol). It indicated that both DVB and EDMA can be selected as crosslinkers. Moreover, the ΔE_2 value between EDMA and MAA was lower than that between DVB and MAA, revealing that EDMA was more suitable as the cross-linking agent for DES-MIPs.

3.5. The nature of the imprinting interaction between DES and MAA

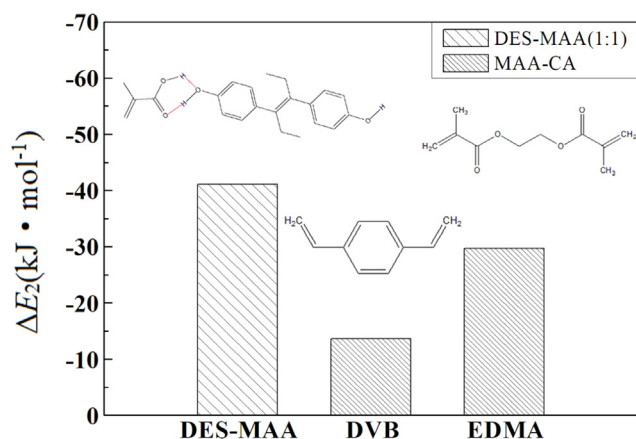
To investigate the nature of the interaction between DES and MAA in the DES-MIPs system, the electron density topological analysis of the complex formed from DES and MAA (1:1) with the lowest binding energy was performed at the LC-

ω PBE/6-31G(*d,p*) level (Lu and Chen, 2012), and its molecular diagram was shown in Fig. 7. Fig. 7 shows that O20 and H21 on the phenolic hydroxyl group in the DES molecule had bond critical point (BCP) with H48 on the hydroxyl group and O46 on the carbonyl group in the MAA molecule, respectively. The BCP connected the two atoms, O20 and H48 as well as H21 and O46, through two bond paths. Thus, the existence of bond paths displayed that there was a bonding interaction between the two atoms, O20 and H48 as well as H21 and O46.

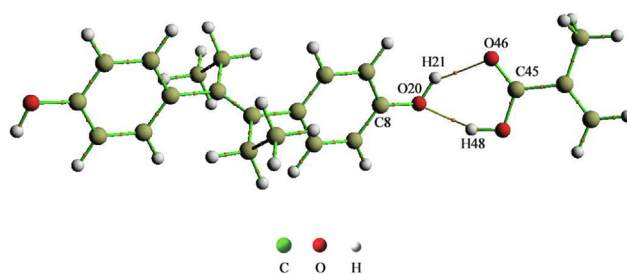
The Atoms in Molecules (AIM) theory can study interactions among many kinds of atoms, especially in hydrogen-bonded systems. According to the AIM theory, the nature of bonding in DES-MAA prepolymers (1:1) can be determined

Table 2 Relevant parameters of the molecularly imprinted interaction system between DES and functional monomers.

Complexes	Number of H-bond	Action sites	H-bond length (nm)	ΔE_1 (kJ/mol)
DES-AM (1:4)	6	C9-H29...O42	0.2450	-86.50
		C7-O19...H44	0.2038	
		O19-H22...N73	0.2041	
		C8-O20...H54	0.2116	
		O20-H21...O52	0.1787	
		C8-O20...H67	0.2398	
DES-APBA (1:4)	6	C8-O20...H74	0.2057	-90.81
		C8-O20...H76	0.2119	
		O20-H21...O91	0.1869	
		O19-H22...O111	0.1885	
		C7-O19...H56	0.2099	
		C7-O19...H58	0.2052	
DES-OPD (1:4)	6	C8-O20...H88	0.2217	-108.17
		O20-H21...N67	0.1814	
		C8-O20...H71	0.2400	
		C7-O19...H53	0.2419	
		O19-H22...N52	0.1814	
		C7-O19...H104	0.2223	
DES-MAA (1:5)	9	C10-H23...O46	0.2451	-146.62
		C8-O20...H48	0.1867	
		C8-O20...H84	0.1955	
		O20-H21...O82	0.1777	
		O19-H22...O94	0.1706	
		C5-H28...O58	0.2399	
		C7-O19...H60	0.1867	
		C7-O19...H72	0.1883	
		C9-H29...O70	0.2320	

**Fig. 6** ΔE_2 between DES and MAA (1:1) as well as MAA and cross-linking agents.

by analyzing the Laplacian value ($\nabla^2\rho(r)_{\text{bcp}}$) and the energy density of electrons (E_{H}) at BCP (Zhang et al., 2019). $\nabla^2\rho(r)_{\text{bcp}}$ value could directly reflect the type of chemical bond. When $\nabla^2\rho(r)_{\text{bcp}}$ is larger than 0, the corresponding chemical bond is a hydrogen bond. The energy density of electrons (E_{H} , $E_{\text{H}} = 0.5 V(r)$) could also indicate the nature of bonding. In theory, the hydrogen bonding energy is larger than -42 kJ/mol. In Table 3, the $\nabla^2\rho(r)_{\text{bcp}}$ values at BCP of the two bonds formed by the DES-MAA (1:1) prepolymer were 0.0919 and 0.0929 a.u., respectively. It satisfied the requirement of hydrogen bonds range for the formation of typical hydrogen bonds proposed by Rozas et al (Rozas et al., 2000). In addition, their

**Fig. 7** Molecular diagram of DES-MAA prepolymer (1:1).

E_{H} values (-30.82 and -33.21 kJ/mol) were larger than -42 kJ/mol, respectively. Aforementioned calculated results indicated that the active sites of interaction between DES and MAA are recognized through hydrogen bonding.

3.6. Preparation of DES-MIPs

According to the predicted results, the DES-MIPs and NIPs microspheres were synthesized at 333 K, when EDMA was the cross-linking agent, acetonitrile was the solvent, and the imprinting ratio between DES and MAA was 1:5. The scanning electron microscopy (SEM) was used to investigate the microsphere morphology, particle size, and distribution range of DES-MIPs and NIPs (Fig. 8). In Fig. 8, the microsphere morphology of MIPs and NIPs were nearly circular in shape, with a more homogeneous morphology and good dispersion. The particle size of microspheres was analyzed using the Nano Measurer 1.2 program (Wang et al., 2021), and the particle

Table 3 $\nabla^2\rho(r)_{\text{bcp}}$ values and E_H values of DES-MAA prepolymer (1:1) at the LC- ω PBE/6-31G(d,p) level.

Molar ratios	Actions sites	$\nabla^2\rho(r)_{\text{bcp}}$ (a.u.)	E_H (kJ/mol)
1:1	C8-O20··H48	0.0919	-30.82
	C45-O46··H21	0.0929	-33.21

diameter ranges of DES-MIPs and NIPs were 105–260 nm and 70–200 nm, respectively. It indicated the synthetic DES-MIPs had internal pores matching with DES when polymerization reaction was carried out. Thus, the internal pores made the particle size of MIPs larger than that of NIPs.

3.7. Optimization of sensor detection conditions

In this study, the PVC embedding method was used to fix DES-MIPs stably on the surface of QCM electrodes. Thus, the amounts of DES-MIPs and PVC affected the number and thickness of the imprinting binding sites of the modified film, which in turn affected the sensitivity and response time of the sensor detection. In Fig. 9, when the pH of the PB background solution was 7 and the coating amount was 5, 10, 15, 20, and 25 μL , respectively, the response frequency of the sensor was increased and then decreased with the increase of the DES-MIPs addition. According to the original measuring curve (Fig. S1, Supporting Information), the response time of the sensor was 24 min. When the amount of polymer addi-

tion was 15 mg, the response frequency of sensor was the maximum and the sensitivity of detection was the highest. This indicates that the excess DES-MIPs would overlap each other, affecting the amount of selective adsorption at the imprinting binding sites. As a result, it would lead to a decrease of response for sensor. When the amount of polymer addition was 15 mg and the coating volume was 5 μL , the imprinting film would be relatively thin. Thus, the binding sites were fewer and the sensor response was weaker. As the coating volume increased, the number of imprinted polymer particles on the modified film also increased, providing more binding sites and increasing the response frequency. The sensor response frequency reached a maximum when the coating volume reached 10 μL , i.e., the adsorption of DES reached saturation. However, when the coating volume was larger than 10 μL , the imprinting film would be relatively thick and the DES-MIPs on the film were densely distributed or even stacked, resulting in the response frequency of the sensor decrease. Moreover, the thick film would lead to the loss of resonance activity of the crystal substrate. Therefore, when the amount of polymer addition was 15 mg and the coating volume was 10 μL , the response frequency of the sensor was the maximum and the detection of DES was most sensitive.

3.8. Selective analysis of sensors

The response frequencies of sensor to DES-acetonitrile standard solution with different concentrations (50–350 ng/mL) were investigated when the amount of polymer addition was

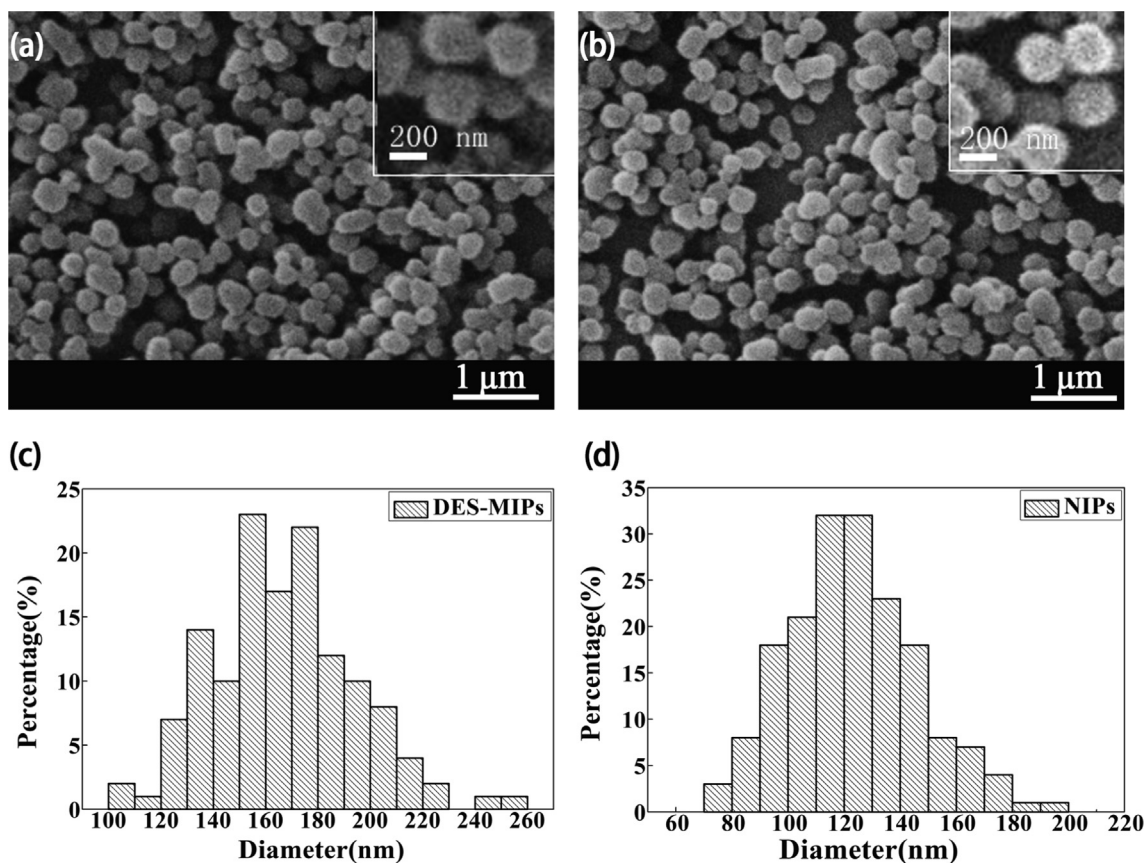


Fig. 8 SEM of DES-MIPs (a) and NIPs (b) and particle size distributions of DES-MIPs (c) and NIPs (d).

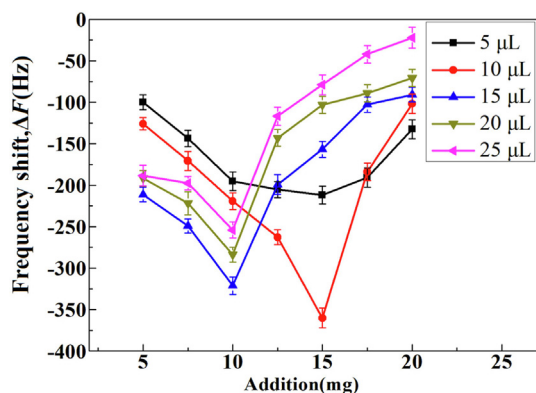


Fig. 9 Frequency shifts of sensor at different amount additions and coating volume of DES-MIPs.

15 mg, coating volume was 10 μL , and pH value of PB solution was 7. Each experiment was repeated three times. The results were shown in Fig. 10(a). The response frequency of sensor increased as the concentration of DES standard solution increased, and the response regression equation of DES-MIPs modified sensor in this detection concentration range was $Y = -1.768X - 15.848$ ($R^2 = 0.9987$). According to the equation, the limit of detection (LOD) was $3.3\delta/S$ (S , slope; δ , residual standard deviation) and the LOD value of the DES-MIPs-modified sensor was 2.63 ng/mL. The LOD value obtained in this study was lower than that of the rapid detection for DES by using the arrayed langasite crystal microbalance (Liu et al., 2017). Moreover, the frequency shifts of the DES-MIPs-modified sensor are much larger than those of the NIPs-modified sensor (Fig. 10(a)).

E3, E1, and BPA were selected as structural analogues of DES to investigate the response frequencies of DES and its structural analogues on sensors, which were constructed with QCM electrodes modified by DES-MIPs. As shown in Fig. 10(b), the response frequencies of the QCM sensor to DES and its structural analogues (E3, E1, and BPA) were in the order of DES > BPA > E3 > E1. The QCM sensor has the best selective recognition and the largest response frequency for DES, which is due to the fact that DES functional groups can interact with the binding sites in the holes of poly-

mer particles on the modified film. In addition, the response frequency of BPA was greater than that of E3 and E1. It may be because that BPA and DES were both phenolic compounds and contained phenol. In contrast, the E1 contained a cyclopentanone ring, which was different significantly from the structure of DES. The selection factor (α) values of the sensors were 1.23, 1.47, and 5.47 for BPA, E3, and E1, respectively. It was shown that the sensor had a strong selectivity for DES when DES coexisted with E1 in the substance to be measured, and all these studies indicate that the DES molecularly imprinted QCM sensor has a better selectivity for DES.

3.9. Application of sensors in the detection of environmental water samples

According to the fitted linear equation, a certain amount of DES solution was added to the water samples, and the response values were detected using the DES-MIPs modified QCM sensor for several cycles to investigate the feasibility and detection rate of the sensor in water sample detection. The results are shown in Table 4. In Table 4, the response frequency value of sample solution was -364.29 Hz for the first time and the corresponding concentration of DES was 197.08 ng/mL in the sample solution. Along with the number of cycles increased, the response frequency of sensor to sample solution decreased. The response frequency value of sample solution was -340.21 Hz for the seventh detection, corresponding to the concentration of DES was 183.46 ng/mL.

Table 4 Cycling performance of the sensor tested in the water samples (200 ng/mL).

Times	Response values (Hz)	Concentrations (ng/mL)	Recovery rates (%)
1	-364.29	197.08	98.54
2	-358.95	194.06	97.03
3	-352.90	190.64	95.32
4	-348.27	188.02	94.01
5	-345.62	186.52	93.26
6	-342.65	184.84	92.42
7	-340.21	183.46	91.73

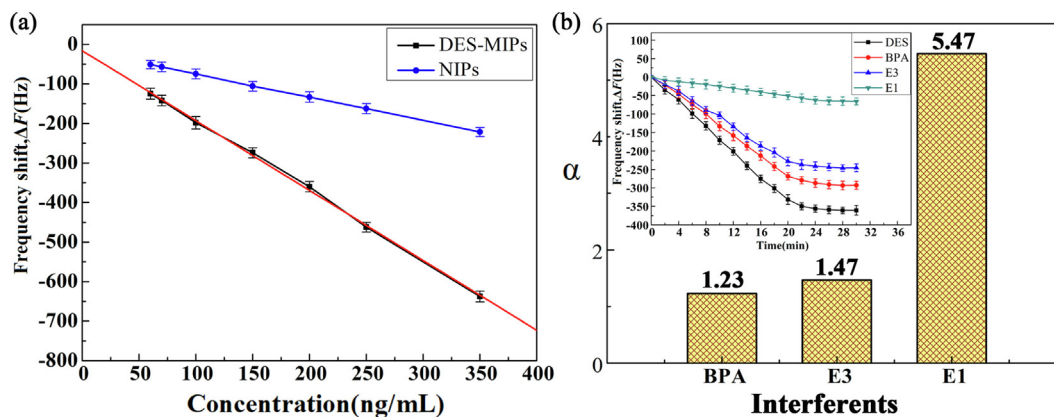


Fig. 10 Frequency shifts of the sensor for different concentrations of DES standard solution (a), the α values of the sensor for BPA, E3, and E1, insert was the respond frequency of sensor for BPA, E3, and E1 and DES (b).

Compared to the original solution concentration (200 ng/mL), the detection range was from 91.73% to 98.54%. It indicated that using DES-MIPs modified QCM sensors to detect water samples is feasible and has stable cycle utilization. However, after seven cycles, the detection rate of QCM sensor was significantly reduced due to more or less damage to the internal pore structure of the DES-MIPs on its surface during electrode cleaning, thus, the error of the detection results will increase. In addition, the response frequency value of actual sample with low concentration of DES standard solution (50 ng/mL) was explored. The recovery rates were between 89.96% and 96.94% (Table S1, [Supporting Information](#)). It indicates that the DES-MIPs modified QCM sensor could also be applied to detect the samples with low concentration.

4. Conclusions

In this study, we investigated the interaction bonding sites, prepolymer spatial configuration, and bonding parameters of DES and four functional monomers using the LC- ω PBE/6-31G(*d,p*) method. The nature of prepolymer interactions and the selection of the best functional monomer and crosslinker were also performed. The calculation results showed that DES-MAA prepolymers interacted with each other through hydrogen bonding. The optimized cross-linking agent was EDMA and the optimized molar ratio between DES and MAA was 1:5 when the solvent was acetonitrile. According to the theoretical results, the QCM sensor was constructed with DES-MIPs modified electrode. The experimental results showed that the maximum response frequency of sensor was obtained when the pH value of PB background solution was 7, the amount of DES-MIPs addition was 15 mg, and the coating volume was 10 μ L. The LOD value of sensor was 2.63 ng/mL. The DES-MIPs-QCM sensor showed good selectivity and recognition of DES among its analogues under optimal detection conditions. In the simulation of real water samples, the recovery rates of DES-MIPs-QCM sensor were ranged from 91.73% to 98.54% for 7 cycles (the concentration of DES standard solution was 200 ng/mL), demonstrating the DES-MIPs-QCM sensor owned good stability and reproducibility.

Declaration of Competing Interest

The authors declare that they have no known competing financial interests or personal relationships that could have appeared to influence the work reported in this paper.

Acknowledgment

The Science and Technology Development Planning of Jilin Province (20200201202JC).

Appendix A. Supplementary material

Supplementary data to this article can be found online at <https://doi.org/10.1016/j.arabjc.2023.104601>.

References

- Aqababa, H., Tabandeh, M., Tabatabaei, M., et al, 2013. Computer-assisted design and synthesis of a highly selective smart adsorbent for extraction of clonazepam from human serum. *Mat. Sci. Eng. C-Mater.* 33 (1), 189–195. <https://doi.org/10.1016/j.msec.2012.08.029>.
- Chi, H., Liu, G., 2022. Determination of acrylamide by a quartz crystal microbalance sensor based on nitrogen-doped ordered mesoporous carbon composite and molecularly imprinted poly (3-thiophene acetic acid) with gold nanoparticles. *Food Control* 141,. <https://doi.org/10.1016/j.foodcont.2022.109166>.
- Craig, Z.R., Keating, A.F., 2022. Editorial - Ovarian toxicants special issue. *Reprod. Toxicol.* 111, 81–82. <https://doi.org/10.1016/j.reprotox.2022.05.011>.
- Czanderna, A.W., Lu, C., 1984. Chapter 1 - Introduction, History, and Overview of Applications of Piezoelectric Quartz Crystal Microbalances. In: Lu, C., Czanderna, A.W. (Eds.), *Methods and Phenomena*. Elsevier, pp. 1–18.
- Eddaif, L., Shaban, A., Telegdi, J., et al, 2020. A piezogravimetric sensor platform for sensitive detection of lead (II) ions in water based on calix[4]resorcinarene macrocycles: Synthesis, characterization and detection. *Arab. J. Chem.* 13 (2), 4448–4461. <https://doi.org/10.1016/j.arabjc.2019.09.002>.
- Fang, G., Liu, G., Yang, Y., et al, 2016a. Quartz crystal microbalance sensor based on molecularly imprinted polymer membrane and three-dimensional Au nanoparticles@mesoporous carbon CMK-3 functional composite for ultrasensitive and specific determination of citrinin. *Sensor. Actuat. B-Chem.* 230, 272–280. <https://doi.org/10.1016/j.snb.2016.02.053>.
- Fang, G., Wang, H., Yang, Y., et al, 2016b. Development and application of a quartz crystal microbalance sensor based on molecularly imprinted sol-gel polymer for rapid detection of patulin in foods. *Sensor. Actuat. B-Chem.* 237, 239–246. <https://doi.org/10.1016/j.snb.2016.06.099>.
- Fang, G., Yang, Y., Zhu, H., et al, 2017. Development and application of molecularly imprinted quartz crystal microbalance sensor for rapid detection of metolcarb in foods. *Sensor. Actuat. B-Chem.* 251, 720–728. <https://doi.org/10.1016/j.snb.2017.05.094>.
- Frisch, M.J., Trucks, G.W., Schlegel, H.B., et al., 2009. Gaussian 09, Revision A.02; Gaussian Inc., Pittsburgh, PA, USA.
- Fuji, S., Tanaka, K., Kishikawa, S., et al, 2022. Quartz crystal microbalance sensor for the detection of collagen model peptides based on the formation of triple helical structure. *J. Biosci. Bioeng.* 133 (2), 168–173. <https://doi.org/10.1016/j.jbiosc.2021.11.006>.
- Giusti, R.M., Iwamoto, K., Hatch, E.E., 1995. Diethylstilbestrol revisited: a review of the long-term health effects. *Ann. Intern. Med.* 122 (10), 778–788. <https://doi.org/10.7326/0003-4819-122-10-199505150-00008>.
- Guo, F., Liu, Q., Qu, G., et al, 2013. Simultaneous determination of five estrogens and four androgens in water samples by online solid-phase extraction coupled with high-performance liquid chromatography-tandem mass spectrometry. *J. Chromatogr. A* 1281, 9–18. <https://doi.org/10.1016/j.chroma.2013.01.044>.
- He, X., Mei, X., Wang, J., et al, 2016. Determination of diethylstilbestrol in seawater by molecularly imprinted solid-phase extraction coupled with high-performance liquid chromatography. *Mar. Pollut. Bull.* 102 (1), 142–147. <https://doi.org/10.1016/j.marpolbul.2015.11.041>.
- Huo, D., Anderson, D., Palmer, J.R., et al, 2017. Incidence rates and risks of diethylstilbestrol-related clear-cell adenocarcinoma of the vagina and cervix: Update after 40-year follow-up. *Gynecol. Oncol.* 146 (3), 566–571. <https://doi.org/10.1016/j.ygyno.2017.06.028>.
- Hu, W.-Y., Kang, X.-J., Zhang, C., et al, 2014. Packed-fiber solid-phase extraction coupled with high performance liquid chromatography-tandem mass spectrometry for determination of diethylstilbestrol, hexestrol, and dienestrol residues in milk products. *J. Chromatogr. B* 957, 7–13. <https://doi.org/10.1016/j.jchromb.2014.02.036>.
- Jiang, W., Yan, Y., Ma, M., et al, 2012. Assessment of source water contamination by estrogenic disrupting compounds in China. *J. Environ. Sci.* 24 (2), 320–328. [https://doi.org/10.1016/S1001-0742\(11\)60746-8](https://doi.org/10.1016/S1001-0742(11)60746-8).
- Jiang, X., Chen, H., Cui, Z., et al, 2016. Low-dose and combined effects of oral exposure to bisphenol A and diethylstilbestrol on the male reproductive system in adult Sprague-Dawley rats. *Environ.*

- Toxicol. Phar. 43, 94–102. <https://doi.org/10.1016/j.etap.2016.02.014>.
- Khan, M.S., Pal, S., Krupadam, R.J., 2015. Computational strategies for understanding the nature of interaction in dioxin imprinted nanoporous trappers. *J. Mol. Recognit.* 28 (7), 427–437. <https://doi.org/10.1002/jmr.2459>.
- Kong, L.-J., Pan, M.-F., Fang, G.-Z., et al, 2014. Molecularly imprinted quartz crystal microbalance sensor based on poly(o-aminothiophenol) membrane and Au nanoparticles for racotopamine determination. *Biosens. Bioelectron.* 51, 286–292. <https://doi.org/10.1016/j.bios.2013.07.043>.
- Latif, U., Qian, J., Can, S., et al, 2014. Biomimetic Receptors for Bioanalyte Detection by Quartz Crystal Microbalance - From Molecules to Cells. *Sensors-Basel.* 14 (12), 23419–23438. <https://doi.org/10.3390/s141223419>.
- Liu, S., Xie, Z., Wu, X., et al, 2005. Separation of structurally related estrogens using isocratic elution pressurized capillary electrochromatography. *J. Chromatogr. A* 1092 (2), 258–262. <https://doi.org/10.1016/j.chroma.2005.08.024>.
- Liu, J., Cai, X., Liu, J., et al, 2022. Study on the Preparation of Estrone Molecularly Imprinted Polymers and Their Application in a Quartz Crystal Microbalance Sensor via a Computer-Assisted Design. *Int. J. Mol. Sci.* 23 (10), 5758. <https://doi.org/10.3390/ijms23105758>.
- Liu, X., Hu, Y., Sheng, X., et al, 2017. Rapid high-throughput detection of diethylstilbestrol by using the arrayed langasite crystal microbalance combined with gold nanoparticles through competitive immunoassay. *Sensor. Actuat. B-Chem.* 247, 245–253. <https://doi.org/10.1016/j.snb.2017.03.014>.
- Lu, T., Chen, F., 2012. Multiwfn: A multifunctional wavefunction analyzer. *J. Comput. Chem.* 33 (5), 580–592. <https://doi.org/10.1002/jcc.22885>.
- Mi, J., Dong, X., Zhang, X., et al, 2019. Novel hapten design, antibody recognition mechanism study, and a highly sensitive immunoassay for diethylstilbestrol in shrimp. *Anal. Bioanal. Chem.* 411 (20), 5255–5265. <https://doi.org/10.1007/s00216-019-01905-z>.
- Nayyar, I.H., Batista, E.R., Tretiak, S., et al, 2011. Localization of Electronic Excitations in Conjugated Polymers Studied by DFT. *J. Phys. Chem. Lett.* 2 (6), 566–571. <https://doi.org/10.1021/jz101740w>.
- Parr, R.G., 1983. Density functional theory. *Annu. Rev. Phys. Chem.* 1 (34), 631–656.
- Qi, P., Xu, Z., Zhou, T., et al, 2021. Study on a quartz crystal microbalance sensor based on chitosan-functionalized mesoporous silica for humidity detection. *J. Colloid. Interf. Sci.* 583, 340–350. <https://doi.org/10.1016/j.jcis.2020.09.029>.
- Rozas, I., Alkorta, I., Elguero, J., 2000. Behavior of Ylides Containing N, O, and C Atoms as Hydrogen Bond Acceptors. *J. Am. Chem. Soc.* 122 (45), 11154–11161. <https://doi.org/10.1021/ja0017864>.
- Sarghein, M.G., Ghiasi, R., Baniyaghoob, S., 2022. Chemisorption C₂H₂ On C₂₀ Bowl: A Computational Investigation. *J. Struct. Chem.* 63 (10), 1600–1609. <https://doi.org/10.1134/S0022476622100067>.
- Sweeney, M.F., Hasan, N., Soto, A.M., et al, 2015. Environmental endocrine disruptors: Effects on the human male reproductive system. *Rev. Endocr. Metab. Disord.* 16 (4), 341–357. <https://doi.org/10.1007/s11154-016-9337-4>.
- Troisi, R., Hatch, E.E., Palmer, J.R., et al, 2018. Estrogen Metabolism in Postmenopausal Women Exposed In Utero to Diethylstilbestrol. *Cancer Epidemiol. Biomark. Prev.* 27 (10), 1208–1213. <https://doi.org/10.1158/1055-9965.EPI-18-0135>.
- Troisi, R., Hatch, E.E., Titus, L., et al, 2019. Prenatal diethylstilbestrol exposure and cancer risk in women. *Environ. Mol. Mutagen.* 60 (5), 395–403. <https://doi.org/10.1002/em.22155>.
- Upton, K., Sathyanarayana, S., Scholes, D., et al, 2015. Early-life factors and endometriosis risk. *Fertil. Steril.* 104 (4), 964–971.e5. <https://doi.org/10.1016/j.fertnstert.2015.06.040>.
- Vydrov, O.A., Scuseria, G.E., 2006. Assessment of a long-range corrected hybrid functional. *J. Chem. Phys.* 125, (23). <https://doi.org/10.1063/1.2409292> 234109.
- Wang, Q., Gu, Y., Li, Q., et al, 2021. Nano-crystalline powders and microwave dielectric properties of Zr_{0.8}Sn_{0.2}TiO₄ ceramics derived using deep eutectic solvents. *J. Mater. Sci. Mater. Electron.* 32 (18), 23317–23324. <https://doi.org/10.1007/s10854-021-06816-3>.
- Yearley, E.J., Zhurova, E.A., Zhurov, V.V., et al, 2008. Experimental electron density studies of non-steroidal synthetic estrogens: Diethylstilbestrol and dienestrol. *J. Mol. Struct.* 890 (1–3), 240–248. <https://doi.org/10.1016/j.molstruc.2008.03.053>.
- Zhang, Q.-L., Li, J., Ma, T.-T., et al, 2008. Chemiluminescence screening assay for diethylstilbestrol in meat. *Food Chem.* 111 (2), 498–502. <https://doi.org/10.1016/j.foodchem.2008.04.010>.
- Zhang, B., Fan, X., Zhao, D., 2019. Computer-Aided Design of Molecularly Imprinted Polymers for Simultaneous Detection of Clenbuterol and Its Metabolites. *Polymers-Basel.* 11 (1), 17. <https://doi.org/10.3390/polym11010017>.